HHS Public Access

Author manuscript

Nat Methods. Author manuscript; available in PMC 2013 September 20.

Published in final edited form as:

Nat Methods. ; 9(5): 480–482. doi:10.1038/nmeth.1955.

Segregation of molecules at cell division reveals native protein localization

Dirk Landgraf[1], **Burak Okumus**[1], **Peter Chien**[2,3], **Tania A. Baker**[2], and **Johan Paulsson**[1]

[1]Department of Systems Biology, Harvard Medical School, Boston, Massachusetts, USA

[2]Department of Biology, Massachusetts Institute of Technology, Cambridge, Massachusetts, USA

[3]Department of Biochemistry and Molecular Biology, University of Massachusetts Amherst, Amherst, Massachusetts, USA

Abstract

We introduce a non-intrusive method exploiting post-division single-cell variability to validate protein localization. The results show that Clp proteases, widely reported to form biologically relevant foci, are in fact uniformly distributed inside *Escherichia coli* cells, and that many commonly used fluorescent proteins (FPs) cause severe mislocalization when fused to homo-oligomers. Re-tagging five other reportedly foci-forming proteins with the most monomeric FP tested suggests the foci were caused by the FPs.

Protein localization measurements increasingly rely on fluorescent protein (FP) fusions, while immunofluorescence – the former gold standard – is being phased out due to labor-intensive procedures, the requirement for antibodies, and the potential for fixation artifacts. In studies of bacterial cells, the convenience of FP fusions quickly led to a sea change, revealing that these cells have a high degree of spatial organization and are far from 'bags of enzymes'[1, 2]. Some of the proteins that were found to be localized are involved in processes like cell division where spatial aspects are central, but many studies[3-5] have reported that numerous other proteins also form foci. However, few localization results have been independently validated. We designed a function-based validation assay for protein localization patterns in live cells and applied it to a canonical example of a bacterial protein reported to form biologically relevant foci across a range of bacterial species: the Clp proteases[3-12].

Conceptually, our approach exploits the fact that localization patterns determine the statistical differences between the two daughter cells right after cell division, and thereby

Correspondence should be addressed to J.P. (Johan_Paulsson@hms.harvard.edu).

Author Contributions: D.L. and J.P designed the study, devised the experimental strategies, interpreted the results, and wrote the paper. D.L. further constructed the plasmids and strains, performed all experiments and analyzed the data. B.O. built the HILO imaging setup, performed the HILO microscopy with D.L. and participated in the writing. P.C. and T.A.B. provided crucial reagents and participated in the discussions and writing.

Competing Financial Interests: The authors declare no competing financial interests.

Note: Supplementary Information is ablvailae on the Nature Methods website.

influence the post-division heterogeneity in any affected downstream processes. By measuring the downstream heterogeneity in the presence and absence of a fluorescent tag to a protein of interest, a side-by-side comparison reveals whether the tag interferes with protein localization; for non-intrusive tags, the post-division single-cell heterogeneity in the downstream process should be the same with or without the FP (Fig. 1a).

We first fused two commonly used FPs, Venus YFP and superfolder GFP (sfGFP), to the ClpX and ClpP proteins in *E. coli* and confirmed the previously reported localization patterns, typically observing a single bright focus in roughly half of the cells during balanced exponential growth in rich media. Cells without a focus exhibit a low cytoplasmic FP signal, similar to the cytoplasmic signal in foci-harboring cells. Tracking cells through division showed how the focus segregated to one of the two daughters, while the other cell formed a new focus within a few generations (Supplementary Video 1 and Supplementary Note 1). The observed localization of the Clp-FP protease foci should thus cause substantial post-division single-cell heterogeneity in the turnover rates of protease substrates.

We then used dual-color time-lapse microscopy to simultaneously measure substrate abundances and protease localization patterns in individual *E. coli* cells over time. As the reporter substrate we fused mCherry to the *E. coli* ssrA tag, which marks mCherry for proteolysis by ClpXP (Fig. 1b) and to a lesser extent by ClpAP[13]. We expressed mCherry-ssrA from an inducible promoter in both foci-forming FP strains and in the wildtype strain and followed the fate of the mCherry-ssrA degradation reporter over time. Specifically, we measured the reporter degradation rate in daughter cells after cell division and analyzed the heterogeneity between individual daughter cell pairs.

When either ClpX or ClpP was tagged with Venus YFP or sfGFP, cells that contained the focus actively degraded mCherry-ssrA, whereas cells without a focus showed mild to extreme reduction in mCherry-ssrA degradation, thus producing two daughters with very different mCherry-ssrA degradation rates (Fig. 1c, Supplementary Video 2 and Supplementary Figure 1). However, both daughter cells in the wildtype strain continued proteolysis of mCherry-ssrA at very similar rates (Fig. 1c, Supplementary Video 3 and Supplementary Fig. 2). This shows that the FP tag causes clustering artifacts, and that the ClpX-FP and ClpP-FP fusions cannot be trusted for determining the localization of the native, untagged proteins.

To further validate our results we performed several independent tests. We used immunofluorescence microscopy against ClpX (Fig. 2a) with the strain expressing the foci-forming ClpX-Venus YFP fusion as a positive control and a ClpX knockout strain as a negative control, confirming that the anti-ClpX antibodies were specific and that fixation did not disassemble the ClpX-Venus YFP foci. In wildtype cells, the immunofluorescence images indicate that ClpX forms 20–50 complexes that are uniformly distributed in the cell. We also used the small monomeric SNAP tag fused to ClpP (Fig. 2b) and ClpX (data not shown), and again observed a uniform spatial distribution of these proteins.

These findings motivated us to evaluate other FPs (Supplementary Table 1) fused to ClpP or ClpX. We found that sfGFP, Venus YFP, mCherry, and mCherry2 all cause substantial foci

formation in the majority of cells, despite being monomers or very weak dimers when expressed alone. mKate2 and TagRFP-T caused intermediate clustering, while for mVenus YFP and mYPet most of the fluorescence signal was spatially uniform, although foci were observed in a few cells. The mTagBFP and mEos2 fusions resulted in a weak signal with infrequent dim foci. We detected no foci for PS-CFP2, rsFastLime (data not shown) and GFP(–30) but the signal was very dim. Finally, mGFPmut3, Dronpa, and Dendra2 displayed an essentially uniform signal. FP fusions to ClpP generally caused more foci formation than fusions to ClpX, in particular for mYPet (Fig. 2d). Because foci-forming tendencies could also be affected by protein expression levels, which in turn could be affected by the FP tags, we expressed two separate copies of the gene for ClpP-mGFPmut3 in the same strain. We observed no increase in clustering despite the higher level (Supplementary Fig. 3 and 4).

We further analyzed the ClpP-SNAP tag, ClpP-Dronpa, ClpP-Dendra2 and ClpP-mGFPmut3 fusions using our single-cell segregation assay and observed very little post-division cell-to-cell variability, confirming that these tags, though not perfectly mimicking the wildtype, are less prone to clustering artifacts (Fig. 3). All ClpP-FP fusions also showed a somewhat reduced degradation activity when compared to the wildtype, presumably because the bulky FP tags interfere with protease activity. Of all the reporters tested, the SNAP tag was both the most active and least intrusive in terms of localization.

Gentle fixation of cells harboring the ClpX-mGFPmut3 and ClpP-mGFPmut3 fusions also revealed uniformly distributed complexes (Fig. 2e,f). We further used HILO microscopy (Online Methods) to perform real-time single-molecule imaging in live cells. ClpA-mGFPmut3, ClpP-mGFPmut3 and ClpX-mGFPmut3 complexes were all observed to move freely and rapidly in the cytoplasm (Fig. 2g, Supplementary Videos 4–7). Individual ClpP-Dronpa molecules could also be detected in live cells with HILO imaging and were also uniformly distributed (Supplementary Fig. 10).

The bright ClpP-FP foci are proteolytically active and highly fluorescent, showing that the fusions are functional and not misfolded. Introducing the monomeric A206K mutation[14] into an FP also substantially reduced foci formation, again demonstrating that the foci are not caused by spontaneously misfolded FPs. Even the strongest foci-forming FPs, like Venus YFP, are spatially uniform when expressed alone, even at high levels (Supplementary Fig. 5). Both the Clp complexes and the FPs are thus spatially uniform on their own, and only form foci when fused to each other. We hypothesize that this is due to avidity effects. In FP fusions, the homo-oligomeric proteins could act as scaffolds, bringing several FPs into close proximity. This would prevent the oligomers from diffusing apart after a single FP-FP dissociation event and allow them to rebind before the remaining links are broken (Fig. 2c), thereby driving the coalescence of tagged oligomers into visible foci.

These results raise the question of how many other reported foci are caused or greatly exaggerated by FP fusions. In fact, the FPs we observed to be prone to clustering are used in the three main bacterial FP fusion libraries – mCherry in *C. crescentus*[5], Venus YFP in *E. coli*[4], and GFPuv4 in the *E. coli* ASKA library[3] – that all report numerous foci. The ClpX and ClpP foci have even been used as positive controls in genome-wide localization studies[5]. To investigate whether FPs cause false localization patterns more generally, we

used one of our most monomeric FPs, mGFPmut3, to re-tag five *E. coli* proteins – Hfq, PepP, IbpA, FruK, and MviM – that previously were reported to form bright foci in multiple FP libraries[3, 4]. Fusions PepP-mGFPmut3, FruK-mGFPmut3, and MviM-mGFPmut3 showed no foci, while Hfq-mGFPmut3 and IbpA-mGFPmut3 were uniformly distributed in most cells and only showed dim foci in a small fraction of cells (Supplementary Fig. 6, Supplementary Video 8 and Supplementary Table 2). Our results strongly suggest that FP-mediated clustering is a widespread phenomenon although further tests, as presented for the Clp proteins, will be necessary to prove this unequivocally.

The segregation-based assay described here cannot be used for all cellular components since we cannot always measure the heterogeneity in an affected downstream process with existing reporters. However, the assay could be used for any factor that directly or indirectly affects transcription, translation, RNA degradation or proteolysis: protein localization patterns can be analyzed with FP reporters and mRNA localization patterns with the MS2 tagging system or FISH (although it should be noted that these patterns themselves may be prone to artifacts). It may also be possible to probe segregation of factors involved in other types of processes, using light microscopy to determine cell morphology, for instance, or using FRET biosensors to measure pH, metabolites, ATP levels or Ca^{2+} ions. Because the assay is based on a relative comparison with and without a tag, it is insensitive to systematic measurement errors and can resolve small statistical differences. For example, if two different FPs produce different localization patterns (as expected from Fig. 2d), testing which FP interferes less with the heterogeneity of a downstream process could suggest which reporter is more trustworthy.

We hope the results described here will lead to a reinvestigation of protein localization in bacteria, that the FP survey will guide the choice of fluorescent reporters both for conventional and super-resolution localization measurements, and that the segregation-based assay will prove useful in other biological systems.

Online Methods

Construction of plasmids and *E. coli* strains

All *E. coli* strains, plasmids and primers are listed in Supplementary Table 3–5, respectively. The strain and plasmid constructions are described in Supplementary Note 2. Various *E. coli* strains with Clp-FP fusions were verified by Western blotting (Supplementary Fig. 7 and 8 and Supplementary Methods 1). The SNAP tag and the FPs used in this study, including their amino acid sequences, are listed in Supplementary Table 1.

Epi-fluorescence and time-lapse microscopy

All epi-fluorescence microscopy experiments were performed on an inverted microscope (Nikon Ti-E) equipped with a Perfect Focus System (PFS, Nikon), an Orca R2 (Hamamatsu) camera, a Scion CFW-1612M (Scion corporation) camera, a 100× Plan Apo objective (NA = 1.4, Nikon), or a 100× TIRF (total internal reflection fluorescence) objective (NA = 1.49, Nikon) and an automated xy-stage (BioPrecision2 Inverted Stage, Ludl). The microscope was controlled by Micro-manager (http://www.micro-manager.org/) and custom-written Matlab scripts. For phase imaging, cells were illuminated with a white LED light source

(pE-100, CoolLED) and high-resolution phase images were captured with the Scion camera (44 nm effective pixel size). Fluorescence imaging was performed with an LED system (Spectra 7 light engine, Lumencor) and appropriate filter cubes: DAPI (LF405-A, Semrock), CFP (CFP-2432A, Semrock), GFP (GFP-3035B, Semrock), YFP (YFP-2427A, Semrock), Cy3 (TRITC-A, Semrock) and RFP (mCherry-A, Semrock). The fluorescence images were captured non-binned with the Orca R2 camera (64.5 nm effective pixel size) and saved as 16-bit TIFF images.

Overnight liquid cultures, started from a single colony, were grown at 30 °C or 37 °C in a shaking incubator. 14–16 h post-inoculation, cells were diluted 1:1,000 into imaging medium (M9 medium with 0.2% (w/v) glucose and 10% (v/v) Luria Bertani (LB) medium). Cells were usually grown until early exponential phase (OD_{600} = 0.1–0.2), diluted with imaging medium and ∼5 μl cell suspension was spotted onto an agar pad. Cells were allowed to sit on the pad for 5–20 min before imaging. The agar pads were made of 2% (w/v) low-gelling agarose (Sigma-Aldrich, A9414 or QA-Agarose, MP Biomedicals, cat# AGAL0050) dissolved in imaging medium. The microscope is equipped with a large incubator and time-lapse imaging was performed at 30 °C or 37 °C. Coverslips were sequentially sonicated for 30 min in 1 M KOH, acetone, 100% ethanol, and ddH_2O, and then extensively rinsed with ddH_2O before use.

For the FP survey, cells were grown at 37 °C to early exponential phase, spotted on an agar pad and then imaged at room temperature (22–26 °C). The strain with the ClpP-mGFPmut3 fusion was grown at 30 °C before imaging. Typical exposure times were 500–2,000 ms for the non-foci forming fusions and 20–2,000 ms for the foci-forming FPs.

Measurement of single-cell degradation rates in daughter cells after cell division

E. coli cultures were grown overnight in LB medium, supplemented with 100 μg/ml ampicillin, at 37 °C in a shaking incubator. 14–16 h post-inoculation, cells were diluted 1:1,000 into imaging medium (without antibiotics), grown for ∼100 min (wake-up from stationary phase), diluted 1:10 and induced for 2 h with 2 mM Isopropylβ-D-1-thiogalactopyranoside (IPTG) to produce the mCherry-ssrA(LAA) tag degradation reporter. After the IPTG induction, cells were pelleted (4,000 g, 2 min, 37 °C), washed 3 times with pre-warmed imaging medium, diluted 1:10 into pre-warmed imaging medium, grown for 15 min (250 rpm, 37 °C), diluted 1:20–1:50 into pre-warmed imaging medium and 2–5 μl cell suspension was spotted on a pre-warmed agar pad. Care was taken to keep the cells at 37 °C during handling and to avoid any temperature changes. The time-lapse experiments were usually started ∼40 min after washing away the IPTG. The microscope was enclosed by an in-house built incubator and imaging was performed at 37 °C (or 30 °C with previous cell growth also at 30 °C and cell handling at room temperature). 5–15 stage positions, each having usually one individual *E. coli* cell, were manually selected (only based on the phase image) and imaged every 5 min in a time-lapse fashion to monitor growth into a micro-colony. A custom-written Matlab script was used to track the micro-colonies during imaging and to correct for xy-drift caused by movement of the agar pad. In short, a 2 × 2 binned phase image was acquired at every time point, segmented to find the micro-colony and the center of the micro-colony was automatically moved to the center of the field of view of the

camera before the acquisition of a phase z-stack (5–6 planes with 0.2 μm spacing) and the fluorescence images. The exposure times for GFP or YFP images were 50–1,000 ms and for RFP images 200 ms. RFP images were taken every time-point with GFP and YFP images (to monitor the protease) being less frequent (e.g. every fifth time point). Dark field images were acquired for all exposure times and subtracted from the respective fluorescence images.

Quantitative image and data analysis was done using the Schnitzcell program[15] (courtesy of Prof. M. Elowitz, Caltech) and Matlab. The *E. coli* cells were segmented based on a 0.2–0.3 μm out-of-focus high-resolution phase image (Supplementary Fig. 9). Cells were tracked for 30 frames at 30 °C or 20 frames at 37 °C (5 min between frames in both cases). Tracking of cells that grow out of the in-focus monolayer of the micro-colony was aborted and those cells were excluded from the analysis. Cell segmentation and cell tracking were manually checked and errors were corrected. Single-cell degradation rates (i.e. the decrease of the total RFP fluorescence intensity per cell over time) were measured in daughter cells after cell division. The reported degradation rates correspond to the average rates during the cell cycle of the daughter cells (i.e. measured from birth to the next division). If one cell divides earlier, the last frame of the earlier dividing daughter cell defines the end point for calculating the average degradation rate of both siblings. Daughter cells with very low mCherry levels (corresponding to cells at the end of the pulse-induction experiment when most of the mCherry-ssrA proteins were degraded) and daughter cells with degradation rates below 10,000 or negative values (due to delayed mCherry maturation at the beginning of the experiment) were excluded from the analysis.

Immunofluorescence microscopy

E. coli cells were grown to early exponential phase (OD_{600} = 0.1–0.15) in LB medium at 30 °C with shaking at 250 rpm. 1 ml of cells was pelleted (4,000 g, 2 min, room temperature), resuspended in 500 μl freshly prepared fixation solution (30 mM sodium phosphate buffer pH 7.4, 2.5% formaldehyde (Ted Pella, cat# 18505)) and incubated for 10 min at room temperature on an inverter followed by 30 min on ice. The cells were pelleted (4,000 g, 2 min, 4 °C) and washed 3 times with 500 μl ice-cold 1× PBS. Cells were pelleted again and incubated for 5 min at room temperature in 25 μl GTE buffer (20 mM Tris-HCl pH 7.5, 50 mM glucose, 10 mM EDTA) supplemented with 2.5 μg/ml lysozyme (Sigma-Aldrich, cat# L6876). After the incubation, the cells were diluted 1:10 with GTE buffer and 10 μl of the cell suspension was spread on a KOH-cleaned coverslip, which was coated with 0.01% poly-lysine solution (Sigma-Aldrich, cat# P8920). The cells were allowed to air-dry (> 30 min). Next, 200 μl blocking buffer (1× PBS, 2% (w/v) BSA, 0.05% (v/v) Tween-20) was added to the coverslip and incubated for 15 min at room temperature. Anti-ClpX antibody (see below) was diluted 1:100 in blocking buffer and each coverslip was incubated with 200 μl antibody solution for 1 h in a homemade humidity chamber. The coverslips were incubated 3 times for 5 min with 200 μl blocking buffer. Secondary antibody (Alexa 350 donkey anti-rabbit IgG (Invitrogen, cat# A10039)) was diluted 1:500 in blocking buffer and ∼300 μl was added to each coverslip. The coverslips were incubated in the dark for 1 h. Next, cells were washed 3 times with 200 μl blocking buffer with 5 min incubations between washes. Coverslips were mounted on agar pads made of 2% low-gelling temperature agarose

(Sigma-Aldrich, A9414) in 1× PBS. The IF samples were imaged on an inverted microscope (Nikon Ti-E) equipped with a 100× TIRF objective (NA = 1.49, Nikon), an Orca-R2 camera (Hamamatsu) and a shuttered mercury light source (Intensilight, Nikon). The Alexa 350 fluorophores were imaged with a DAPI (LF405-A, Semrock) filter cube.

Anti-ClpX antibody

Antibodies to ClpX were purified using Affigel-10 (Bio-Rad) resin. The *E. coli* ClpX protein was purified according to previous protocols[16], conjugated to resin, and ClpX polyclonal rabbit antibodies (Covance) were purified according to the manufacture's protocol. Affinity-purified antibodies were aliquoted in 1× PBS containing 50% glycerol and stored at −80°C.

SNAP tag labeling in fixed *E. coli* cells

The SNAP tag[17] (NEB) has not previously been used to detect endogenous intracellular proteins in bacteria and hence the existing protocols needed to be carefully optimized. The ClpP-SNAP tag strain and the wildtype strain, which served as a negative control to demonstrate the specificity of the labeling reaction, were processed in parallel and subjected to identical treatments. First, *E. coli* cells were grown to mid-exponential phase in LB medium at 37 °C with shaking (250 rpm). Cells were fixed with 2.5% (v/v) formaldehyde by adding 1.56 ml of a 16% formaldehyde solution (Ted Pella, cat# 18505) directly to 8.44 ml cell culture and incubated at room temperature for 30 min in a shaking incubator (250 rpm). After fixation, the cell suspension was pelleted by centrifugation (4,000 g, 10 min, 4 °C), washed with 2 M glycine to quench the fixation reaction and incubated in 1 ml 2 M glycine for 1 h in a thermomixer (Eppendorf) at room temperature with 1,400 rpm shaking. The 1 h incubation with 2 M glycine reduced the non-specific binding of the TMR SNAP-Cell dye[18]. The SNAP-Cell TMR dye (NEB, S9105S) was diluted in DMSO (Sigma-Aldrich, cat# D2650) to a final concentration of 30 μM and used as a 100× stock. After the 1 h glycine incubation, cells were pelleted (4,000 g, 2 min, room temperature), washed with 1 ml washing buffer (1× PBS, 200 mM glycine, 1 mM DTT, 2% (w/v) BSA, 0.05% (v/v) Tween-20) and incubated in the thermomixer for 10 min (1,400 rpm, room temperature). Cells were then pelleted again and concentrated in 100 μl washing buffer, followed by the addition of 1 μl 30 μM SNAP-Cell TMR dye and incubated for 30 min in the thermomixer (1,400 rpm, room temperature). The labeling reaction and all the following steps were done under low-light conditions. After incubation with the TMR dye, cells were subjected to excessive washing steps to remove non-specifically bound dye molecules. The cells were pelleted (4,000 g, 2 min, room temperature) and were washed ∼10 times with 1 ml wash buffer and incubated for ∼1 h between washes in the thermomixer (1,400 rpm, room temperature). The progression of the washing was monitored by observing the sample and the negative control side-by-side. Before microscopy, cells were washed twice with 1× PBS, diluted with 1× PBS (if necessary) and imaged on an agarose pad (2% (w/v) low-gelling agarose dissolved in 1× PBS) or squashed between a coverslip, coated with 0.01% poly-L-lysine (Sigma-Aldrich, cat# P8920), and a microscope slide.

Imaging was performed with an inverted microscope (Nikon Ti-E) equipped with an Orca R2 (Hamamatsu) camera, a Spectra 7 light engine (Lumencor) and a 100× Plan Apo

objective (NA = 1.4, Nikon). The TMR-stained bacteria were imaged with the green LED (excitation filter 549/15 nm, 40 mW power measured out of the objective) and a Cy3 filter cube (TRITC-A, Semrock) with typical exposure times of 2–5 s.

Highly inclined and laminated optical sheet (HILO) microscopy

Cells were grown at 30 °C or 37 °C to exponential phase and the microscopy was performed at room temperature. Bacteria were imaged via an in-house built objective-type TIRF-based configuration on a modified inverted microscope (Nikon Ti-E) equipped with a 100× Plan Apo objective (NA = 1.4, Nikon) and a 2.5× C-mount adapter (Nikon). Illumination was achieved by a 488 nm (Sapphire, Coherent) laser line, which was focused on the back focal plane of the objective. Since TIRF modality does not allow the whole bacterial cell volume to be illuminated, the laser light was diverted from TIRF and sent to the sample at an inclined fashion[19], i.e. with an angle that is slightly steeper than the critical angle. The incidence angle was adjusted manually by varying the position of the focusing lens sitting on an xyz stage (Newport) and was empirically optimized for the best signal-to-noise ratio. Images were acquired using an electron-multiplying CCD camera (ixon3 897, Andor) with EM gain set to 300 and a 5× pre-amplifier gain. The camera was controlled with the software Solis (Andor). The effective pixel size of the acquired images corresponds to 64 nm (250× magnification). To acquire fast dynamics only a sub-region of the EMCCD chip was used. ClpA-mGFPmut3, ClpX-mGFPmut3, ClpP-mGFPmut3 and mGFPmut3 alone live-cell movies were acquired under constant illumination with 10 mW laser intensity and 30 Hz image acquisition rate. For GFP imaging, a dichroic filter (Di01-R488, Semrock) and a bandpass emission filter (FF01-525/45, Semrock) were mounted on a custom-made brass filter cube.

The image sequences were exported from Solis as 16-bit TIFF files and cropped to 128 × 128 pixel in ImageJ (NIH, http://rsbweb.nih.gov/ij/). The images were then loaded into Matlab for batch processing and intensity scaled. For quantitative intensity scaling, all images in a movie sequence have the same grayscale scaling, where the pixel with the highest numerical value in the image sequence corresponds to the white pixel (1) and the pixel with the lowest numerical value to the black pixel (0). For “per frame auto-scaling”, every image in the sequence is subjected to an individual min/max scaling, where the brightest pixel in the individual image corresponds to the white pixel (1) and the pixel with the lowest numerical value to the black pixel (0). The resulting images were loaded into QuickTime 7 Pro (version 7.6.6, Apple) and compressed with the H.264 codec.

The images for the live-cell HILO time-series (Fig. 2g) were acquired similarly except with 150× magnification and a Hamamatsu EMCCD camera (C9100-02) with an effective pixel size of 53.3 nm and 50 EM gain. Images in sequence were acquired every second with 20 ms exposure time and shuttered 15 mW 488 nm laser illumination in HILO mode.

Short fixation of cells containing the ClpP-mGFPmut3 or ClpX-mGFPmut3 fusion

Exponential phase cells, harboring the ClpP-mGFPmut3 or ClpX-mGFPmut3 fusion, were grown in imaging medium, spun down (4,000 g, 2 min, 4 °C) and resuspended in 1 ml fixation solution (2.5% formaldehyde, 30 mM sodium phosphate buffer pH 7.4) and

incubated for 5 min on ice. Cells were pelleted and washed with 1 M glycine, followed by three washes with 1× PBS. Finally, the cells were squashed between a KOH-cleaned coverslip and a microscope slide and imaged immediately with the same setup that was used for live-cell HILO microscopy. Image sequences were acquired with constant illumination using 30 ms integration time and 30 mW (ClpX-mGFPmut3, Fig. 2e) or 10 mW (ClpP-mGFPmut3, Fig. 2f) 488 nm laser intensity. The EM gain was set to 50 and 5× pre-amplifier gain was used. The TIFF image sequences were loaded into ImageJ to generate sum projections of the first 100 (ClpX-mGFPmut3) or 300 (ClpP-mGFPmut3) frames.

Supplementary Material

Refer to Web version on PubMed Central for supplementary material.

Acknowledgments

We are grateful to D. Rudner, T. Mitchison and M. El Karoui for valuable comments on the manuscript. We thank E. Toprak for help with instrumentation, M. Elowitz (Caltech) for providing image analysis tools, P. Malkus for various plasmids, N. Lord for assistance with Tn7 integration, and A. Hilfinger and D. Huh for discussions. We are also indebted to the Harvard Medical School Nikon Imaging Center and the developers of Micro-manager. This work was supported by the US National Institutes of Health Grants GM081563 and GM095784.

References

1. Rudner DZ, Losick R. Cold Spring Harb Perspect Biol. 2010; 2:a000307. [PubMed: 20452938]
2. Shapiro L, McAdams HH, Losick R. Science. 2009; 326:1225–1228. [PubMed: 19965466]
3. Kitagawa M, et al. DNA Res. 2005; 12:291–299. [PubMed: 16769691]
4. Taniguchi Y, et al. Science. 2010; 329:533–538. [PubMed: 20671182]
5. Werner JN, et al. Proc Natl Acad Sci U S A. 2009; 106:7858–7863. [PubMed: 19416866]
6. Kain J, He GG, Losick R. J Bacteriol. 2008; 190:6749–6757. [PubMed: 18689476]
7. Winkler J, et al. EMBO J. 2010; 29:910–923. [PubMed: 20094032]
8. Simmons LA, Grossman AD, Walker GC. J Bacteriol. 2008; 190:6758–6768. [PubMed: 18689473]
9. Kirstein J, Strahl H, Moliere N, Hamoen LW, Turgay K. Mol Microbiol. 2008; 70:682–694. [PubMed: 18786145]
10. Dziedzic R, et al. PLoS One. 2010; 5:e11058. [PubMed: 20625433]
11. McGrath PT, Iniesta AA, Ryan KR, Shapiro L, McAdams HH. Cell. 2006; 124:535–547. [PubMed: 16469700]
12. Kirstein J, Moliere N, Dougan DA, Turgay K. Nat Rev Microbiol. 2009; 7:589–599. [PubMed: 19609260]
13. Farrell CM, Grossman AD, Sauer RT. Mol Microbiol. 2005; 57:1750–1761. [PubMed: 16135238]
14. Zacharias DA, Violin JD, Newton AC, Tsien RY. Science. 2002; 296:913–916. [PubMed: 11988576]
15. Rosenfeld N, Young JW, Alon U, Swain PS, Elowitz MB. Science. 2005; 307:1962–1965. [PubMed: 15790856]
16. Levchenko I, Seidel M, Sauer RT, Baker TA. Science. 2000; 289:2354–2356. [PubMed: 11009422]
17. Juillerat A, et al. Chem Biol. 2003; 10:313–317. [PubMed: 12725859]
18. Klein T, et al. Nat Methods. 2011; 8:7–9. [PubMed: 21191367]
19. Tokunaga M, Imamoto N, Sakata-Sogawa K. Nat Methods. 2008; 5:159–161. [PubMed: 18176568]

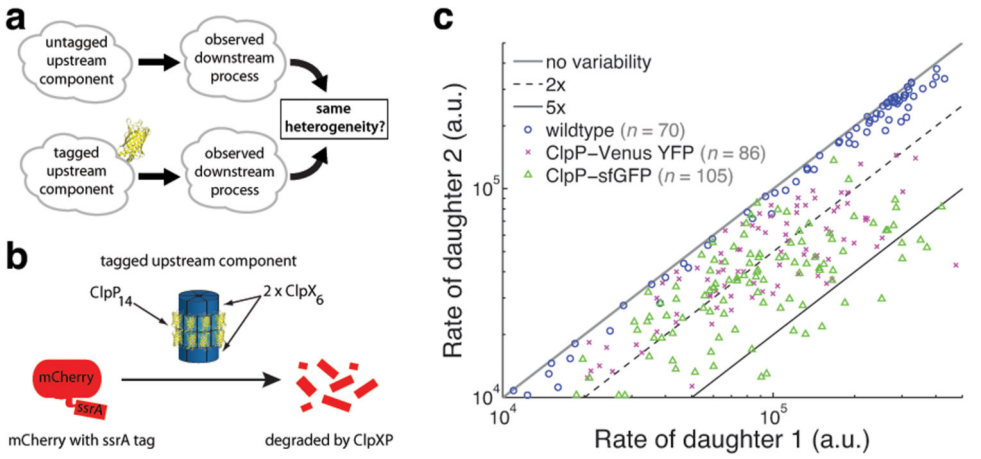

Figure 1.

(**a**) Schematic depiction of the segregation assay. An upstream process (Clp protease localization) affects a downstream process (substrate degradation) that can be measured in daughter cells originating from cells with and without an FP tag on the upstream component. If the tag is non-intrusive, heterogeneity of the downstream process in the daughter cells should be independent of the tag. (**b**) Schematic of the mCherry-ssrA degradation reporter. (**c**) The plot shows single-cell degradation rates as measured by time-lapse fluorescence microscopy in daughter cells after cell division in the indicated bacterial strains. The daughter with the faster degradation rate is plotted on the x-axis. The spread along the diagonal is due to pulse-induction of the mCherry-ssrA reporter. Diagonal lines represent no cell-to-cell variability (gray line), 2× variability (dashed black line) and 5× variability (solid black line). Degradation rates are in arbitrary units (a.u.).

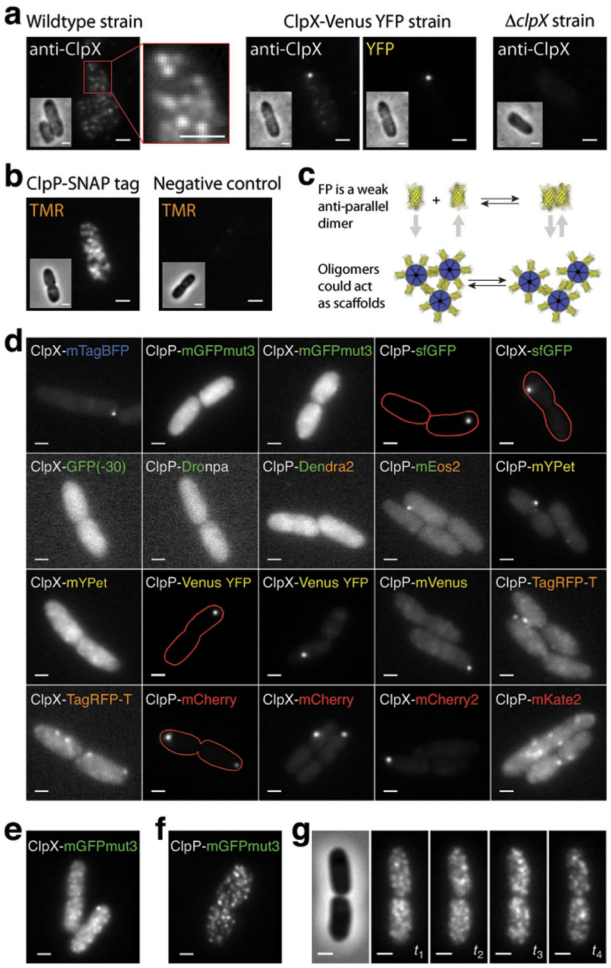

Figure 2.

(**a**) Immunofluorescence microscopy of ClpX in wildtype (left), ClpX-Venus YFP (middle) and Δ*clpX* (right) strains. Insets are phase images and a close-up is shown for the wildtype. (**b**) Fluorescence images show bacteria expressing the ClpP-SNAP tag labeled with TMR (tetramethylrhodamine), compared to wildtype (right). Insets show phase images. (**c**) Cartoons of a fluorescent protein (yellow) forming a weak anti-parallel dimer and of avidity effects potentially clustering tagged ClpX hexamers (blue). (**d**) Fluorescence images of bacteria expressing the indicated constructs. The cell outline (red) is shown for cells with weak cytoplasmic signal. (**e,f**) HILO microscopy of gently fixed cells with ClpX-mGFPmut3 (**e**) and ClpP-mGFPmut3 (f). (**g**) Live-cell HILO microscopy of cells expressing ClpP-mGFPmut3. Scale bars,1 μm.

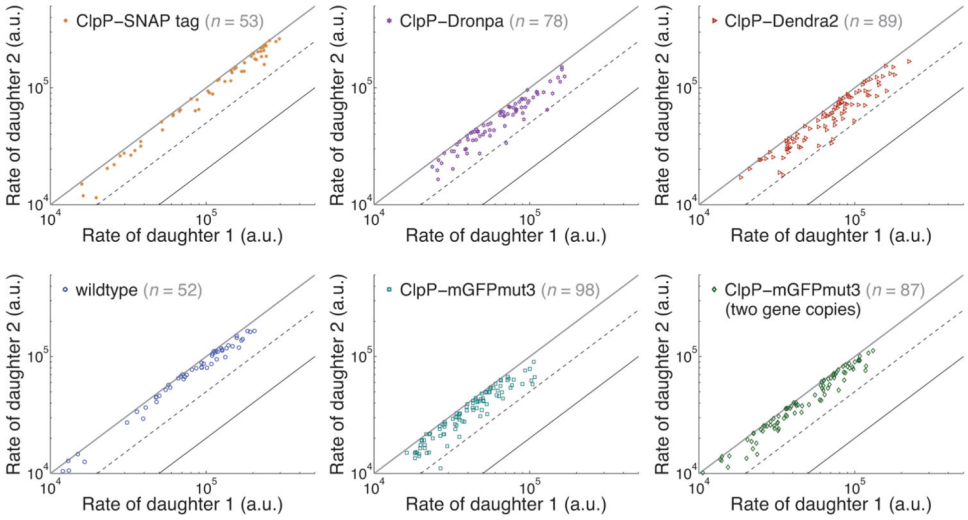

Figure 3.

The plots show single-cell segregation assays for bacteria expressing the indicated proteins. Post-division single-cell degradation rates were measured by time-lapse fluorescence microscopy at 37 °C (upper row) and 30 °C (lower row) for both daughter cells. The ClpP-mGFPmut3 strain, the wildtype and a foci-forming control (Supplementary Fig. 11) were imaged at 30 °C because ClpP-mGFPmut3 levels were reduced at 37 °C but similar to the wildtype at 30 °C (Supplementary Fig. 3). Diagonal lines represent no cell-to-cell variability (gray line), 2× variability (dashed black line) and 5× variability (solid black line). Degradation rates are in arbitrary units (a.u.).